

Monitoring and Targeting Anti-VEGF Induced Hypoxia within the Viable Tumor by ^{19}F -MRI and Multispectral Analysis



Yunzhou Shi^{*}, Jason Oeh[†], Anna Hitz[†],
Maj Hedehus^{*}, Jeffrey Eastham-Anderson[‡],
Franklin V. Peale Jr.[‡], Patricia Hamilton[†],
Thomas O'Brien[†], Deepak Sampath[†] and
Richard A.D. Carano^{*}

^{*}Department of Biomedical Imaging, Genentech Inc., South San Francisco, CA; [†]Department of Translational Oncology, Genentech Inc., South San Francisco, CA; [‡]Department of Pathology, Genentech Inc., South San Francisco, CA

Abstract

The effect of anti-angiogenic agents on tumor oxygenation has been in question for a number of years, where both increases and decreases in tumor $p\text{O}_2$ have been observed. This dichotomy in results may be explained by the role of vessel normalization in the response of tumors to anti-angiogenic therapy, where anti-angiogenic therapies may initially improve both the structure and the function of tumor vessels, but more sustained or potent anti-angiogenic treatments will produce an anti-vascular response, producing a more hypoxic environment. The first goal of this study was to employ multispectral (MS) ^{19}F -MRI to noninvasively quantify viable tumor $p\text{O}_2$ and evaluate the ability of a high dose of an antibody to vascular endothelial growth factor (VEGF) to produce a strong and prolonged anti-vascular response that results in significant tumor hypoxia. The second goal of this study was to target the anti-VEGF induced hypoxic tumor micro-environment with an agent, tirapazamine (TPZ), which has been designed to target hypoxic regions of tumors. These goals have been successfully met, where an antibody that blocks both murine and human VEGF-A (B20.4.1.1) was found by MS ^{19}F -MRI to produce a strong anti-vascular response and reduce viable tumor $p\text{O}_2$ in an HM-7 xenograft model. TPZ was then employed to target the anti-VEGF-induced hypoxic region. The combination of anti-VEGF and TPZ strongly suppressed HM-7 tumor growth and was superior to control and both monotherapies. This study provides evidence that clinical trials combining anti-vascular agents with hypoxia-activated prodrugs should be considered to improved efficacy in cancer patients.

Neoplasia (2017) 19, 950–959

Introduction

The effect of anti-angiogenic agents on tumor oxygenation has been in question for a number of years. A significant number of studies have shown increased tumor hypoxia after administration of antibodies to vascular endothelial growth factor (VEGF) [1–4], whereas other studies have demonstrated a decrease in tumor hypoxia (increased $p\text{O}_2$) [5–7]. This dichotomy in results may be explained by the role of vessel normalization in the response of tumors to anti-angiogenic therapy: anti-angiogenic therapies may initially improve both the structure and the function of tumor vessels, but, sustained or more potent anti-angiogenic treatments can produce an anti-vascular response resulting in vessel pruning and a more hypoxic environment [8]. Regional hypoxia is one of the most important factors regulating tumor growth as well as influencing the clinical outcome after therapeutic intervention [9–11]. Anti-VEGF induced

hypoxia has been proposed as a possible escape mechanism from therapies that block VEGF's actions [12,13] and these therapeutically induced hypoxic regions make a logical target to prevent escape [13].

Abbreviations: VEGF-A, Vascular endothelial growth factor A; TPZ, Tirapazamine; MS, Multispectral analysis; MRI, Magnetic resonance imaging; R_1 , Spin-lattice, or longitudinal, relaxation rate; EC50, Half maximal effective concentration; PFC, Perfluorocarbon; KM, K-means; SVM, Support vector machines; GP, Genetic programming

Address all correspondence to: Richard A. D. Carano, Genentech, Inc., 1 DNA Way, South San Francisco, CA 94080.

E-mail: carano.richard@gene.com

Received 26 May 2017; Revised 18 July 2017; Accepted 24 July 2017

© 2017 The Authors. Published by Elsevier Inc. on behalf of Neoplasia Press, Inc. This is an open access article under the CC BY-NC-ND license (<http://creativecommons.org/licenses/by-nc-nd/4.0/>).

1476-5586

<https://doi.org/10.1016/j.neo.2017.07.010>

Given the importance of hypoxia in tumor biology, anti-VEGF induced hypoxia needs to be more completely understood to better assess monotherapy and combination therapy approaches with antiangiogenic agents.

Quantification of tumor regional hypoxia, both spatially and temporally, is difficult due to the need for a non-invasive technique and the complications arising from heterogeneity in tumor morphology. Recently, a multispectral (MS) ^{19}F -MRI approach has been introduced to provide a means to measure pO_2 within the viable tumor and address the issue of tumor heterogeneity that complicates pO_2 tumor imaging [4]. In addition, this methodology was shown to provide sufficient sensitivity to assess the effects of anti-vascular agents on tumor oxygenation [4]. ^{19}F -MRI oximetry [14–18], which uses perfluorocarbon emulsions (PFCs) as an imaging contrast agent, is a noninvasive method to spatial map tumor pO_2 *in vivo*. These PFCs remain in the tumor and can provide serial pO_2 estimates over an extended period of time without the need for additional administration of PFCs [4,14]. The technique is based on the principle that the spin–lattice, or longitudinal, relaxation rate (R_1) of certain PFCs varies linearly with oxygen levels at a given temperature. This provides ^{19}F -MRI oximetry with the advantageous feature that the pO_2 measurement is independent of the absolute ^{19}F signal intensity (PFCs uptake). Spatial heterogeneity of tumor perfusion and metabolism contribute to regional hypoxia and the heterogeneous tissue morphology of solid tumors [10]. To address tumor heterogeneity, Shi et al. developed a novel approach that combines ^{19}F -MRI R_1 mapping with a diffusion-based multispectral (MS) analysis approach as a means to spatially map *in vivo* pO_2 within the viable tumor, the tissue of therapeutic interest [4].

The initial goal of this study was to employ MS ^{19}F -MRI to quantify pO_2 as a means to evaluate the ability of a high dose of anti-VEGF to produce a strong and prolonged anti-vascular response that results in significant tumor hypoxia. To address this question, an antibody that blocks both murine and human VEGF-A (B20.4.1.1) was evaluated by MS ^{19}F -MRI. B20.4.1.1 has been previously shown to reduce vascular density [19], but provided a somewhat variable response in reducing pO_2 in a murine xenograft tumor model [4]. For this study, the dose of B20.4.1.1 was increased three-fold relative to the previous study as a means to improve the anti-vascular and resultant pO_2 responses. The second major goal of this study was to target the anti-VEGF induced hypoxic tumor micro-environment with an agent, tirapazamine (TPZ), designed to target the hypoxic regions of a tumor [20–22]. TPZ is a member of a class of hypoxia-selective cytotoxins that have been developed to target hypoxic regions of tumors [23]. TPZ (3-amino-1,2,4-benzotriazine 1,4 dioxide, SR4233) is a bioreductive agent selectively toxic to hypoxic cells [20–22]. Clinical evaluation of TPZ has been extensive and includes several positive phase I and II studies [23]. But, these positive early studies were followed by several unsuccessful phase III clinical trials [23]. Despite the lack of phase III success, TPZ remains a very potent molecule to target hypoxic tissue, where it has been reported to be 25 to 200 fold more toxic to cells under hypoxic conditions in culture relative to normoxic conditions [20,22]. TPZ has been recently proposed as an attractive agent to target anti-VEGF induced hypoxia [13]. In this current study, the selective toxicity of TPZ for hypoxic cells was confirmed in a series of *in-vitro* studies and then a series of xenograft tumor model experiments was performed to evaluate the utility of TPZ, used in combination with anti-VEGF, as a means to target the hypoxic viable tumor produced by anti-VEGF therapy.

Materials and Methods

TPZ *In Vitro* Studies

The *in vitro* cell analysis was carried out in a panel of cancer cell lines, including the human colorectal carcinoma HM-7 cell line, the human non-small cell lung carcinoma H1299 cell line, the human colorectal adenocarcinoma HT29 cell line, and the radiation-induced mouse fibrosarcoma-1 (RIF-1) cell line. The different cell lines were selected as representatives of various kinds of cancer types. All cell lines were obtained from in-house tissue culture cell bank, where ATCC (Rockville, MD) was the original source for the HM-7, H1299 and HT29 cell line. The RIF-1 cell lines were obtained from Stanford University through a materials transfer agreement. Cell lines were authenticated by short tandem repeat and genotyped upon re-expansion. Cells were maintained in RPMI 1640 (Sigma-Aldrich, Stockholm, Sweden) medium supplemented with 10% FBS (Sigma-Aldrich, Stockholm, Sweden), and then plated in 96-well black clear bottom Corning CellBIND plate (Sigma-Aldrich, CLS3340-50EA) using RPMI supplemented with 5% FBS, 100 $\mu\text{g}/\text{ml}$ penicillin, 100 units/ml streptomycin (Gibco 15,140–122). The following day, cells were treated with Tirapazamine (Sigma-Aldrich, Stockholm, Sweden) using a six-point dose titration scheme. On Day 5, cell viability was assessed using the CellTiter-Glo (CTG) (Promega, Madison, WI) Luminescence Cell Viability assay using the manufacturer's standard protocol. Half maximal effective concentration (EC50) values were calculated using four-parameter logistic curve fitting. Cell growth was also assessed using live cell imaging with an IncuCyte Zoom (Essen BioSciences, Ann Arbor, MI).

For hypoxic treatments, 24 h after plating, cells were transferred to a BioSpherix hypoxic chamber (XVIVO G300C, Parish, NY) and grown at 37°C , 0.5% O_2 , 5% CO_2 . The O_2 level was independently monitored by a Fibrox3 fiber optic oxygen meter (PreSens Precision Sensing GmbH, Regensburg, Germany).

For the glucose treatments, low glucose medium contained 2 mM glucose (Sigma-Aldrich, Stockholm, Sweden), and high glucose medium contained 10 mM glucose.

Perfluorocarbon Emulsions Preparation

Perfluoro-15-crown-5-ether (SynQuest Laboratories, Inc., Alachua, FL) was mixed with an emulsifying solution of lecithin soy (MP biomedical, Solon, OH) and lactated Ringers solution (Baxter, Deerfield, IL). The mixture was processed using a microfluidizer (LV1, Microfluidics, Newton, MA) at 30000 psi to form emulsions with a diameter of 250 nm, as measured by dynamic light scattering (DynaPro Nanostar, Wyatt Technology, Santa Barbara, CA). The final concentration of perfluoro-15-crown-5-ether was 60 w/v%. The PFCs solutions were then sterilized by microfiltration using membrane filters with a pore size of 0.45 μm and adjusted to a pH of 7.4.

Animal Preparation

The Institutional Animal Care and Use Committee (IACUC) at Genentech Inc. approved all animal protocols in this study. Female athymic nude mice ($n = 92$, 20 to 25 g; Harlan Laboratories, Indianapolis, IN) were inoculated subcutaneously on the hind-limb with HM-7 colorectal cancer cells (3.5×10^6 cells per mouse). The animals that were used in the study had an approximate tumor volume range of 150 to 250 mm^3 (volume = $0.5 \times \text{length} \times \text{width}^2$, assessed by caliper measurements) at the time when the animals

entered the study. For the 7-day efficacy studies, percent tumor growth inhibition (TGI) was calculated at the end of drug treatment on Day 7 using the following formula: $\%TGI = 100 \times ((\text{mean tumor volume in the vehicle treated group at Day 7} - \text{mean tumor volume of drug treated group at Day 7}) / \text{mean tumor volume of vehicle treated group at Day 7})$. For MS ^{19}F -MRI, animals were injected i.v. with 400 μL of the PFC solution at 48 hours and 24 hours prior to MRI.

Mice were placed under anesthesia for preparation for MRI studies by administration of 2% isoflurane in a warm anesthesia induction box, transferred to a custom-built animal holder, and moved to the magnet bore, where anesthesia was maintained with 1% to 2% isoflurane that was adjusted according to the respiration rate of the animal. The animals' breathing rate was monitored and temperature was maintained at 37°C using warm air flow controlled by a LabVIEW software module with feedback provided by a rectal temperature probe (SA Instruments, Stony Brook, NY).

MRI Measurements

Experiments were performed on a 9.4 T Agilent MRI system equipped with a $^1\text{H}/^{19}\text{F}$ 10 mm surface coil (Agilent Technologies Inc., Santa Clara, CA). ^1H -MRI measurements were performed first. Twelve 1-mm thick coronal slices were acquired (field of view (FOV) = 25.6 \times 25.6 mm, matrix = 64 \times 64). A diffusion-weighted fast spin echo multislice (FSEMS) sequence was used to acquire data to calculate ADC maps with the following parameters: 6 b-values ranging from 270 to 1000 s/mm^2 , repetition time (TR) = 3 s, echo train length (ETL) = 4, echo spacing (ESP) = 3.95 ms, number of average (NA) = 2, diffusion gradient separation (Δ) = 30 ms and duration (δ) = 3.3 ms, total scan time 9 minutes. A spin-echo multislice (SEMS) sequence was used to generate T_2 and M_0 maps that employed the following parameters: echo times (TE) = 5, 26, 47, 68 ms, TR = 3 seconds, NA = 1, scan time 12 minutes. Spatial maps of ADC were obtained from the diffusion data by applying a linear least-squares regression to the natural logarithm of the signal intensity. Similarly, T_2 and M_0 maps were obtained from the T_2 -weighted, spin echo data by a linear least-squares regression [24].

^{19}F -MRI was then carried out (FOV = 25.6 \times 25.6 mm, matrix = 32 \times 32, zero-filled to 64 \times 64). A ^{19}F -weighted SEMS sequence was used to obtain a fluorine anatomical reference image (TR = 5 s, TE = 8.5 ms, NA = 4, scan time 10 minutes). A ^{19}F single-shot, inversion recovery FSEMS sequence was employed to generate spatial maps of R_1 (FSEMS, inversion times (TI) = 0.1, 0.3, 0.5, 0.6, 0.7, 0.9, 1.2, 1.8, 2.5 s, TR = 6 s, ESP = 4.1 ms, ETL = 32, NA = 32, scan time 29 minutes). Then, the R_1 of the ^{19}F nucleus was calculated by using the following equation [25]:

$$I(\text{TI}) = I_0 \times (1 - a \times e^{-R_1 \times \text{TI}}) \quad (1)$$

where $I(\text{TI})$ is the signal intensity at time TI, I_0 is the signal intensity at equilibrium magnetization, a is a coefficient, R_1 is the spin-lattice relaxation rate. R_1 , a , and I_0 are determined from Equation (1) using a nonlinear regression algorithm. The pO_2 was then determined according to the calibration curve between R_1 and pO_2 that was previously developed [4].

Multispectral Analysis

Multispectral analysis of the ^1H data was used for tissue segmentation. K-means (KM) clustering was performed using the ADC, proton density and T_2 maps as previously described [24,26,27]. The KM algorithm segmented the tumors into four

tissue classes: viable tumor tissue, sub-cutaneous adipose tissue, a low- T_2 necrotic class (necrosis 1) and a high-ADC necrotic class (necrosis 2). The low- T_2 necrotic class represents active or recent hemorrhage, and the high-ADC necrotic class has been found to represent an acellular, "cyst-like" region [24]. The viable tumor tissue class map was combined with the ^{19}F pO_2 map to estimate pO_2 within the viable tumor.

Histological Analysis

After the final imaging time point, the animals were euthanized by cervical dislocation under anesthesia. The tumors were extracted and fixed in 10% neutral buffered formalin solution. Hematoxylin and eosin (H&E), MECA-32 and Gamma-H2AX (combination study only) stains were used to identify tissue architecture, blood vessels and DNA damage, respectively. Histological viable tumor tissue was identified by H&E staining.

Whole slide images were acquired by the Olympus Nanozoomer automated slide scanning platform (Hamamatsu, Bridgewater, NJ) at 200 \times final magnification. Scanned slides were analyzed in the Matlab software package (version R2016a by Mathworks, Natick, MA) as 24-bit RGB images. Various tumor regions (viable area, necrotic area, and Gamma-H2AX positive cells) were identified using a combination of Support Vector Machines (SVM) [28] and Genetic Programming (GP) [29]. A training set of representative areas was first generated manually and assigned a binary classification (positive for the region of interest or negative for regions to exclude). Then, a SVM was trained using RGB and texture values from these selections. Application of this SVM resulted in a binary image for each selection, the noise in the resulted images was removed through the application of GP, which found a sequence of simple morphological operators that maximized the solution accuracy for both positive and negative selections, which was then applied to the entire image.

The analysis of vascular density was restricted to viable tumor tissue. A segmentation algorithm utilizing a sequence of morphological operations to consolidate MECA-32 stained areas into individual vessels. The identification of vessels was aided by including vessel lumens, as characterized by empty white space that are adjacent to MECA-32 stained regions. Size and shape based filtering of the resulting objects was utilized to remove noise. The vessel density here was defined as percent vessel area (100 \times vessel area divide by viable tumor area). Individual cells were identified using an algorithm based on radial symmetry [30]. Each cell was then scored as positive or negative for Gamma-H2AX staining.

Experimental Protocols

TPZ In Vitro Study

Cells were maintained in RPMI 1640 and then plated in 96-well at the optimal seeding density for 24 hours. The optimal seeding densities were established for each cell line in order to reach 75% to 80% confluence at the end of the assay without treatments.

In the study to determine TPZ EC50 under normoxia and hypoxia conditions, after 24 hours, HM-7, H1299, HT29 and RIF-1 cells were separated into two groups, group 1 cells continued to grow within the same cell incubator, while group 2 cells were transferred to a BioSpherix hypoxic chamber and grown at 37°C, 0.5% O_2 , 5% CO_2 . Both groups were treated with TPZ using a 6-point dose titration scheme. On Day 5, cell viability was assessed to calculate EC50 values.

Since cell metabolism may also be affected by glucose, the second study was carried out on HM-7 and HT29 cells to determine the treatment effect of TPZ under 4 different glucose and oxygenation combinations: normoxia and low glucose, hypoxia and low glucose, normoxia and high glucose, hypoxia and high glucose. TPZ were applied at concentrations of 0 μ M, 0.2 μ M, 2 μ M and 20 μ M, respectively. Cell viability was determined using the Celltiter-Glo (Promega, Madison, WI) luminescent cell viability assay.

All the *in vitro* studies were done in duplicates. The *in vitro* study to assess EC50 was repeated 3 times, and the *in vitro* study to assess glucose and hypoxia effect was repeated 2 times.

High-Dose Anti-VEGF In Vivo MS ¹⁹F-MRI Study Using the HM-7 Colorectal Cancer Xenograft Model

In the high-dose anti-VEGF treatment study, B20.4.1.1 (30 mg/kg, n = 12) or a control antibody (30 mg/kg, n = 12) was administered as a single i.p. dose. MS ¹⁹F-MRI was performed pre-treatment (Day 0) and 24, 48, and 72 hours post treatment (Day 1, Day 2, and Day 3).

Anti-VEGF and TPZ Combination *In Vivo* Studies Using the HM-7 Colorectal Cancer Xenograft Model:

Two 7-day combination studies were performed. The first study was a non-imaging efficacy study where tumor growth was assessed by caliper measurements. The second study was an MS ¹⁹F-MRI efficacy study. Both studies were dosed as follows:

Control group: Vehicle (saline, 200 μ l, IP, BID \times 7 + control antibody 10 mg/kg, 100 μ l, IP, bi-weekly)

B20.4.1.1 group: B20.4.1.1 at 30 mg/kg (loading dose), 5 mg/kg, 100 μ l, IP, bi-weekly + saline 200 μ l, IP, BID \times 7.

TPZ group: TPZ at 10 mg/kg, 200 μ l, IP, BID \times 7, + control antibody, 10 mg/kg, 100 μ l, IP, bi-weekly

Combination group: B20.4.1.1 at 30 mg/kg (loading dose), 5 mg/kg, 100 μ l, IP, bi-weekly + TPZ at 10 mg/kg, 200 μ l, IP, BID \times 7.

Group sizes were set as follows:

Non-imaging efficacy study: n = 10 per group

MS ¹⁹F-MRI efficacy study: control group (n = 8), B20.4.1.1 group (n = 9), TPZ group (n = 7), combination group (n = 10).

Statistical Analysis

Statistical significance was defined as $P < .05$. To compare two groups, an unpaired t-test was used; for three or more groups, a comparison with control was performed using the Dunnett's Test for multiple comparisons. To compare pre-treatment to post-treatment data within a group, a paired t-test was used. Statistical analysis was performed with JMP 9 (SAS Institute, Cary, NC) and Excel 2010 (Microsoft, USA). All data is presented as mean \pm standard error unless otherwise noted.

Results

MS ¹⁹F-MRI Monitors a Sustained Decrease of pO₂ After High-Dose Anti-VEGF Treatment with B20.4.1.1

The ability of a neutralizing antibody to produce a strong hypoxic response in tumors was evaluated in the HM-7 human colorectal cancer xenograft model since it is a highly vascularized tumor model, sensitive to anti-angiogenic agents, and has been previously shown to be responsive to a neutralizing antibody to rodent and human VEGF-A (B20.4.1.1) [4,19,31]. The HM-7 model is a rapidly growing model with a tumor doubling time of approximately 2.5 days when implanted in the hind leg

[4,19]. MS ¹⁹F-MRI was employed to quantify pO₂ as a means to evaluate the ability of a high dose of B20.4.1.1 to produce a strong and prolonged anti-vascular response that results in significant tumor hypoxia. In this study, a high dose of B20.4.1.1 suppressed viable tumor growth and reduced pO₂ within the viable tumor (Figure 1A). A 30 mg/kg dose of B20.4.1.1 produced a significant reduction in viable tumor growth (percent change Day 1 versus Day 0 = 16 \pm 8.3%, $P < .01$; Day 2 versus Day 0 = 28.9 \pm 15.1%, $P < .01$; Day 3 versus Day 0 = 91.7 \pm 25.7%, $P < .05$, Figure 1B) relative to the growth observed in the control group (percent change Day 1 versus Day 0 = 50.7 \pm 8.8%, Day 2 versus Day 0 = 119.4 \pm 18.8%, Day 3 versus Day 0 = 170.9 \pm 29.4%). In addition, B20.4.1.1 treated tumors exhibited a reduction of viable tumor pO₂ with respect to its pre-treatment levels for Day 1 ($\Delta_{\text{Day1-Day0}} = -8.4 \pm 1.7$ mmHg, $P < .01$), Day 2 ($\Delta_{\text{Day2-Day0}} = -13.3 \pm 2.2$ mmHg, $P < .01$) and Day 3 ($\Delta_{\text{Day3-Day0}} = -13.2 \pm 2.5$ mmHg, $P < .01$), and, in comparison with the control group by Day 3 (Control: $\Delta_{\text{Day3-Day0}} = -0.8 \pm 4.5$ mmHg, $P < .05$) (Figure 1C).

Histology Confirms that High-Dose Anti-VEGF Treatment Produced a Strong Anti-Vascular Response

The reduction of pO₂ in viable tumor in the B20.4.1.1 group was likely due to a strong reduction in vascular density that was confirmed by MECA-32 staining. The B20.4.1.1 treated group exhibited a 44% decrease in vascular density (1.7 \pm 0.3%, $P < .05$, Figure 1D) relative to vascular density detected in the control group (3.0 \pm 0.4%). This reduction in vascular density is visually apparent in the example MECA-32 stained sections provided in Figure 1, E and F.

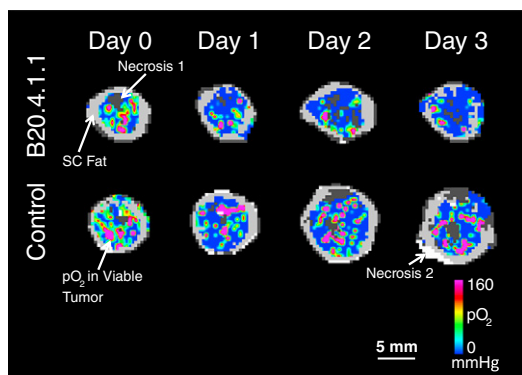
TPZ Was Found to Have Greater Potency Under Hypoxic Conditions

The increase in tumor hypoxia produced by Anti-VEGF treatment provides a potential therapeutic avenue for an agent that targets a hypoxic environment. TPZ has been previously shown to selectively target hypoxic cells [20,21]. A series of *in-vitro* studies were conducted to evaluate the performance of TPZ in four tumor cell lines (HM-7, H1299, HT29, and RIF-1) under normoxia and hypoxia (Figure 2, A-D). The mean ratio of E50 values for TPZ obtained under normoxia versus hypoxia demonstrates that TPZ is highly more potent under hypoxic conditions (HM-7: 5.8, H1299: 7.3, HT29: 10.1, RIF-1: 11.7) (Figure 2D). Nutrient deprivation is another potential consequence of anti-vascular therapies, and, thus, HM-7 and HT29 cells were also evaluated under low and high glucose levels along with hypoxia. There were no observable differences in TPZ potency based on glucose level (Figure 2, E and F). Overall, this data demonstrates that TPZ is well suited to target tumor hypoxia and the HM-7 tumor cell line is suitable for *in-vivo* combination studies.

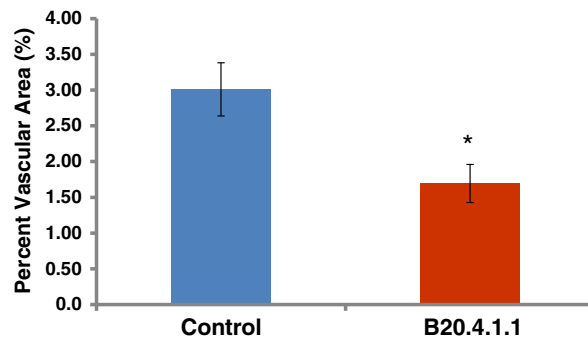
TPZ and Anti-VEGF Used in Combination Produce a Strong Suppression of Tumor Growth

Given that TPZ is dramatically more potent in hypoxic environments, TPZ was used in combination with B20.4.1.1 as a means to target the hypoxic environment created by the anti-vascular effects of B20.4.1.1 treatment. TPZ and B20.4.1.1 were evaluated as single agents and in combination in the HM-7 tumor model by manual caliper measurements. Twice daily IP administration of TPZ at a maximum tolerated dose of 10 mg/kg for 7 days was efficacious in the HM-7 xenograft model and resulted in 49% TGI (tumor volume at end of treatment, Control: 956.2 \pm 122.0 mm³; TPZ: 487.1 \pm 110.3 mm³, $P < .01$, Figure 3A). B20.4.1.1 produced 65% TGI as a single agent after 7 days of treatment (B20.4.1.1: 348.6 \pm 35.8 mm³,

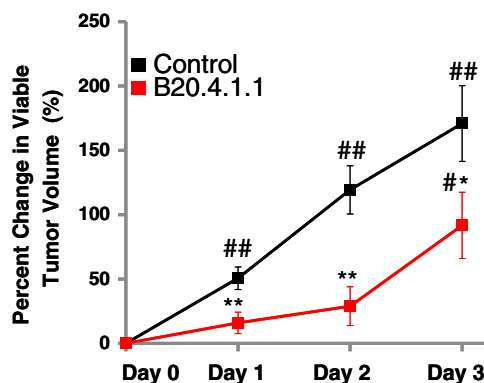
A.



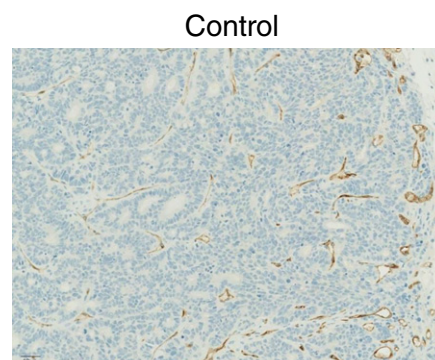
D.



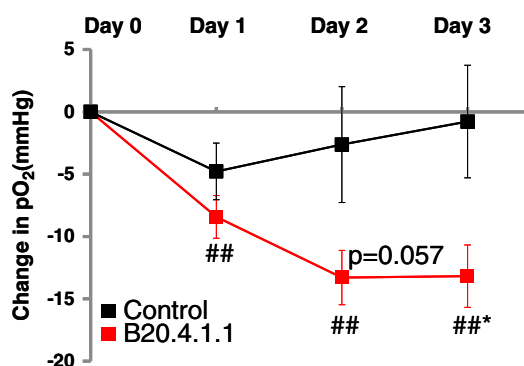
B.



E.



C.



F.

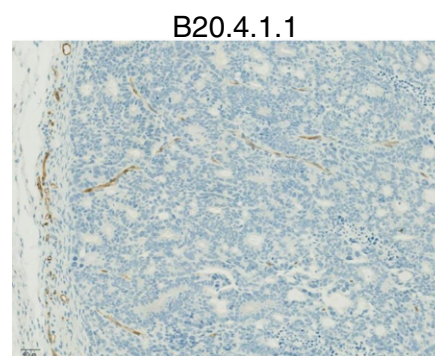


Figure 1. Tumor hypoxia induced by a high dose of B20.4.1.1. (A) Color-coded viable tumor pO_2 maps are superimposed on the corresponding MS tissue class maps for representative animals from each treatment group (pre, 1, 2, and 3 days post treatment). The tissue classes found in the MS tissue class map are gray scale encoded as follows: dark gray – necrosis 1; light gray – subcutaneous adipose tissue; white – necrosis 2; viable tumor – underlies the color-coded viable tumor pO_2 map. (B) The percent change in viable tumor volume as measured by multispectral MRI. Under the treatment of B20.4.1.1, the growth of viable tumor was significantly suppressed as compared to the control group. (C) The pO_2 measured using ^{19}F -MRI. The pO_2 in viable tumor class decreased significantly in the B20-treated group on Day 3 as compared to the control group. (D) Vascular density assessed by MECA-32 histological staining. B20.4.1.1 significantly reduced the percentage of percent vascular area. (E) A representative MECA-32 histology image of the control group, vasculature staining shown in brown. (F) A representative MECA-32 histology image of the B20.4.1.1 group. # $P < .05$ relative to pre-treatment level, ## $P < .01$ relative to pre-treatment level. * $P < .01$ relative to control, ** $P < .01$ relative to control.

$P < .0001$). Combination treatment with TPZ and B20.4.1.1 produced 78% TGI (Combo group: $212.3 \pm 21.2 \text{ mm}^3$, $P < .0001$) relative to control. In addition, combination therapy also suppressed tumor growth relative to B20.4.1.1 ($P < .01$) and TPZ ($P < .05$) monotherapies. There was no significant weight loss over the 7 days of this study (Figure 3B), although there was a downward trend in the TPZ groups at Day 3.

Anti-VEGF and Anti-VEGF + TPZ Groups Exhibited a Significant Increase in Tumor Hypoxia at 48 Hours Post-Treatment

In order to better understand the superiority of combination therapy (B20.4.1.1 + TPZ) over monotherapy with B20.4.1.1 or TPZ, MS ^{19}F -MRI was employed in a imaging efficacy study to evaluate oxygenation within the viable tumor after initiation of therapy. B20.4.1.1 and TPZ were evaluated as single agents and in

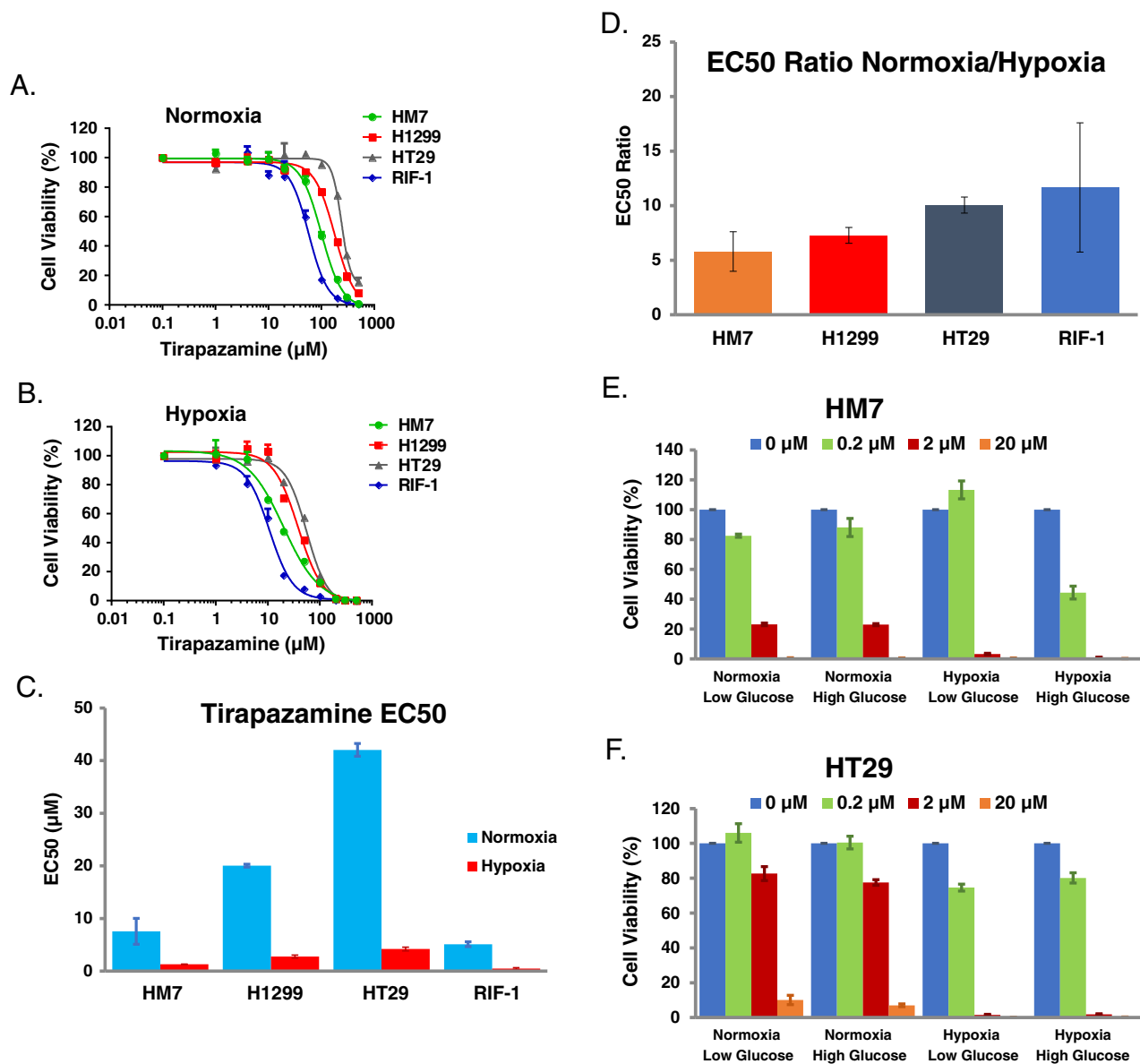


Figure 2. Cell viability *in vitro* is reduced under hypoxia treated by TPZ, but TPZ response is not altered by glucose concentration. (A) HM-7, H1299, HT28 and RIF-1 cell viability under normoxia treated by TPZ, measured by CellTiter-Glo (CTG) luminescence cell viability assay. (B) The same treatment under hypoxia. (C) The comparison of EC50 values under normoxia versus hypoxia condition. (D) The ratio of EC50 values between normoxia and hypoxia. (E) Cell viability as a function of oxygenation and glucose concentration for HM-7 cells under TPZ treatment. (F) Cell viability as a function of oxygenation and glucose concentration for HT29 cells under TPZ treatment. Data in 2C-2F are presented as mean \pm standard deviation.

combination for the HM-7 tumor model. Both the B20.4.1.1 and combination treatment produced a decrease in viable tumor pO_2 , relative to pre-treatment levels, following the onset of treatment (Figure 4, A and B). In the B20.4.1.1 treated group, the change in pO_2 in the viable tumor on Day 2 ($\Delta_{\text{Day2-Day0}} = -14.2 \pm 2.4$ mmHg, $P < .01$) was significantly reduced relative to the changes observed in the control group at Day 2 ($\Delta_{\text{Day2-Day0}} = -3.3 \pm 3.4$ mmHg) and relative to baseline levels ($P < .01$). Combination therapy ($\Delta_{\text{Day2-Day0}} = -13.3 \pm 3.2$ mmHg, $P < .01$) also produced a significant reduction in viable tumor pO_2 relative to the changes observed in the control group at Day 2 and relative to baseline levels ($P < .01$). This reduction in pO_2 is likely driven by B20.4.1.1

treatment since TPZ ($\Delta_{\text{Day2-Day0}} = -0.7 \pm 4.1$ mmHg, $P > .05$) monotherapy did not alter tumor oxygenation.

TPZ and Anti-VEGF Used in Combination Strongly Suppresses Growth of Viable Tumor as Assessed by MS MRI

The increase in viable tumor hypoxia (reduced pO_2) produced by B20.4.1.1 combined with TPZ's ability to target hypoxic tumor cells likely contributed to the strong suppression of viable tumor growth produced by combination treatment with TPZ and B20.4.1.1 (Figure 4, A and C). The percent change (Day 7 versus Day 0) in viable tumor volume was suppressed by TPZ + B20.4.1.1 combination treatment ($49.2 \pm 38.6\%$, $P < .0001$) relative to growth observed in the control

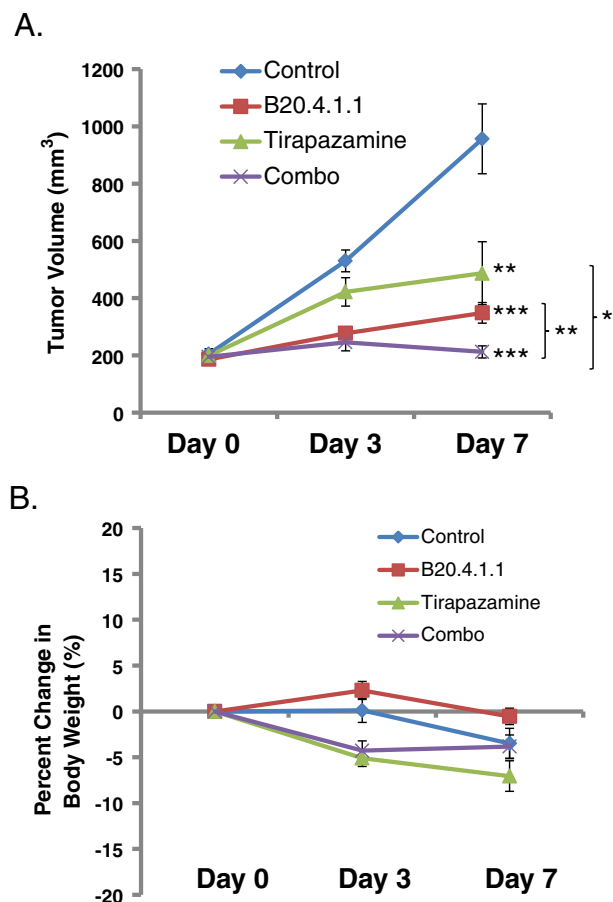


Figure 3. TPZ and Anti-VEGF used in combination produced a strong suppression of tumor growth. (A) At Day 7 post treatment, significant reduction of tumor volume was seen in B20.4.1.1 group, TPZ group and combo group as measured by caliper. Tumor volume for the combo group was also significantly reduced relative to the monotherapy groups. (B) Percent change in body weight over the 7-day study. * $P < .05$, ** $P < .01$, *** $P < .0001$ with respect to control (Dunnett's).

group ($534.1 \pm 60.4\%$) after 7 days of treatment. TPZ + B20.4.1.1 combination treatment also strongly suppressed viable tumor growth relative to the growth observed in the TPZ ($260.9 \pm 69.6\%$, $P < .05$) and B20.4.1.1 ($173.6 \pm 36.5\%$, $P < .05$) monotherapy groups at Day 7. The B20.4.1.1 ($P < .001$) and TPZ ($P < .01$) monotherapy arms did exhibit reduced growth of the viable tumor relative to changes observed in the control group following 7 days of treatment.

Histology Confirms That Combination Therapy Produced a Strong Anti-Vascular and Anti-Tumor Response

Combination therapy with B20.4.1.1 and TPZ produced a significant anti-vascular and anti-tumor response. Combination therapy ($1.0 \pm 0.1\%$, $P < .0001$) produced a 68% reduction in vascular density relative to the control group ($3.2 \pm 0.4\%$) (Figure 5A). B20.4.1.1 monotherapy ($1.1 \pm 0.1\%$, $P < .0001$) produced a similarly strong anti-vascular response, whereas TPZ ($2.8 \pm 0.1\%$, $P > .05$) did not have a significant effect on the tumor vasculature. Gamma-H2AX staining was used to assess DNA damage as a means to determine the anti-tumor effects of B20.4.1.1 and TPZ therapies. Combination therapy with B20.4.1.1 and TPZ was the only therapy regime that produced a significant

Gamma-H2AX response. Combination therapy ($41.5 \pm 4.2\%$, $P < .01$) produced an 84% increase in Gamma-H2AX staining relative to the control group ($22.6 \pm 3.9\%$) (Figure 5B). Neither TPZ ($38.2 \pm 5.1\%$, $P = .06$) or B20.4.1.1 ($24.2 \pm 4.2\%$, $P > .05$) monotherapies produced a significant increase in Gamma-H2AX response, although TPZ exhibited a strong trend. Representative stained sections are shown in Figure 5 for the MECA-32 analysis (Figure 5, C–F) and Gama-H2AX analysis (Figure 5, G–J).

Discussion

This is the first study to employ MS ¹⁹F-MRI pO₂ imaging to confirm that an anti-VEGF therapy can produce a consistent hypoxic response within viable tumor and that this hypoxic tumor tissue can be successfully targeted by a therapy designed to be effective in hypoxic tumor tissue. A high (30 mg/kg) dose of a neutralizing antibody of VEGF was shown to produce a strong hypoxic response in a HM-7 xenograft tumor model (Figure 1, A and C) that was consistent with the strong anti-vascular response confirmed by histology (Figure 1, D–F). The decision to dose B20.4.1.1 at 30 mg/kg was based on a variable pO₂ response observed when B20.4.1.1 was previously dosed at 10 mg/kg in this model [4]. Empirically, the dose was increased three-fold as a means to maximize the anti-vascular response. This increase in B20.4.1.1 dose to 30 mg/kg produced an anti-vascular response that was superior to the previous two studies [4].

This anti-VEGF-induced hypoxic response creates the possibility that therapies designed to target hypoxic regions of a tumor may combine well with anti-vascular therapies. TPZ is a therapy that has been designed to target the hypoxic regions of a tumor, where this bioreductive agent is selectively toxic to hypoxic cells [20,21]. The selective toxicity of TPZ for hypoxic cells was confirmed in a series of *in-vitro* studies in four tumor cell lines (Figure 2, A–F). The ratio of normoxic to hypoxic EC50 values ranges between 5.8 and 11.7 in the four cell lines, demonstrating as expected that TPZ has greater potency under hypoxic conditions. Although this increase in potency for TPZ under hypoxic conditions is below the 25- to 200-fold increase that has been reported in the literature [20,22]. These differences may be due to differences in the choice of cell lines and differences in assay methodology.

Given the confirmation that TPZ provides a means to selectively target hypoxic tumor cells, TPZ and anti-VEGF were evaluated in combination in the HM-7 xenograft tumor model. The monotherapies both demonstrated single agent activity by suppressing tumor growth (Figure 3: tumor volume, Figure 4, A and C: MS viable tumor volume) 7 days post initiation of treatment. The combination therapy of TPZ + anti-VEGF demonstrated a strong reduction in tumor growth that was significantly reduced relative to control and both monotherapy arms (Figs. 3, 4A and C). The imaging study also confirmed that pO₂ was significantly reduced in the anti-VEGF and combination groups after 2 days of treatment (Figure 4, A and B). Histological analysis showed reduced vascular density in the anti-VEGF and combination groups and a significant elevation in gH2A levels for only the combination group at Day 7 (Figure 5B). The elevation in gH2A levels for the combination group is consistent with greater TPZ activity when used in combination with anti-VEGF.

The improved response of the combination group is consistent with greater TPZ activity due to an increase in hypoxia produced by the anti-vascular effects of anti-VEGF and detected by MS ¹⁹F-MRI (reduced pO₂). An alternative explanation is that the improved TPZ

response could be due to improved TPZ delivery given the potential for vascular normalization produced by anti-VEGF [8], leading to increased perfusion and greater TPZ delivery. Improved perfusion, due to vascular normalization, is unlikely to have occurred in this study given the results of this study and previous published results obtained with anti-VEGF in this HM-7 xenograft model [19,26,32]. In the combination treatment MS ¹⁹F-MRI imaging study (Figs. 4 and 5), anti-VEGF reduced pO₂ at 2 days post treatment and was shown to have reduced vascular density at Day 7. In

addition, the high-dose anti-VEGF monotherapy study showed that pO₂ was suppressed at 24, 48 and 72 hours post treatment relative to pre-treatment estimates and reduced vascular density at 72 hours (Figure 1A and C). These data are consistent with a suppression of vascular perfusion by anti-VEGF and not vascular normalization. Previous studies have shown reduced tumor perfusion and vascular density by anti-VEGF in this HM-7 model [26,32]. Berry et al. found that anti-VEGF suppressed the dynamic-contrast-enhanced MRI (DCE-MRI) parameter, K^{trans}, 24 hours after treatment in the HM-7 model, which is consistent with a suppression of perfusion and permeability [26]. O'Connor et al. found that blood volume assessed by dynamic-contrast enhanced ultrasound (DCE-U/S) was reduced by anti-VEGF in this same HM-7 model [32]. These studies were performed with an anti-VEGF antibody, G6-31, that has been shown to perform similarly in the HM-7 model to the antibody, B20.4.1.1, employed in this study [31]. The suppression of tumor perfusion produced by these antibodies is associated with a reduction in vascular density in the HM-7 model at 24 and 48 hours after treatment [4,19,27,32]. Given these data, anti-VEGF at the doses (greater or equal to 5 mg/kg) employed in these studies produces an anti-vascular response in the HM-7 model leading to reduced perfusion, and, thus, it is highly unlikely that TPZ delivery was enhanced due to anti-VEGF treatment.

TPZ demonstrated moderate single agent activity in the HM-7 model (Figs. 3 and 4). This is consistent with the nature of the HM-7 model, which is a rapidly growing model and contains significant regions of the viable tumor that are hypoxic [4], and, thus, making it susceptible to TPZ treatment. TPZ treatment did not alter pO₂ in the viable tumor or vascular density (Figs. 4B, and 5A). TPZ has been shown to exhibit properties similar to a vascular disruption agent when dosed at high levels [33]. A single dose of TPZ at 60 mg/kg was found to increase a histological vascular dysfunction score obtained 24 hours after dosing, whereas, 40 mg/kg was not different from control [33]. There is no evidence of vascular disruption in this current study and this may be due to fact that animals were treated at a much lower dose (10 mg/kg BID) for 7 days. The maximum tolerated dose for 7 days of BID dosing was found to be 10 mg/kg (data not shown).

This is the first study to employ a hypoxia-activated prodrug to target hypoxic regions produced by an anti-vascular agent and identified by MS ¹⁹F-MRI pO₂ imaging. This study demonstrated that an anti-vascular agent (anti-VEGF), given at an initial high dose, can produce a strong, sustained, hypoxic response. This anti-VEGF induced hypoxic region can then be targeted with a therapy (TPZ) that has been designed to treat hypoxic regions of solid tumors. In this study, combination therapy (anti-VEGF + TPZ) resulted in im-

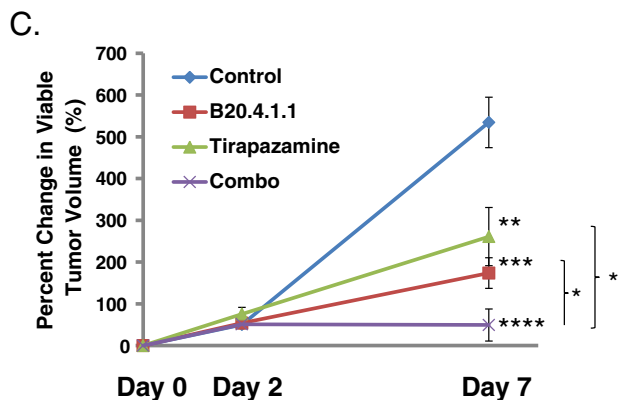
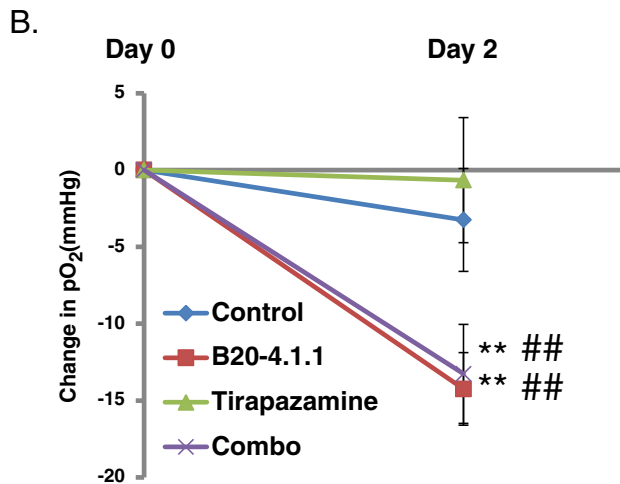
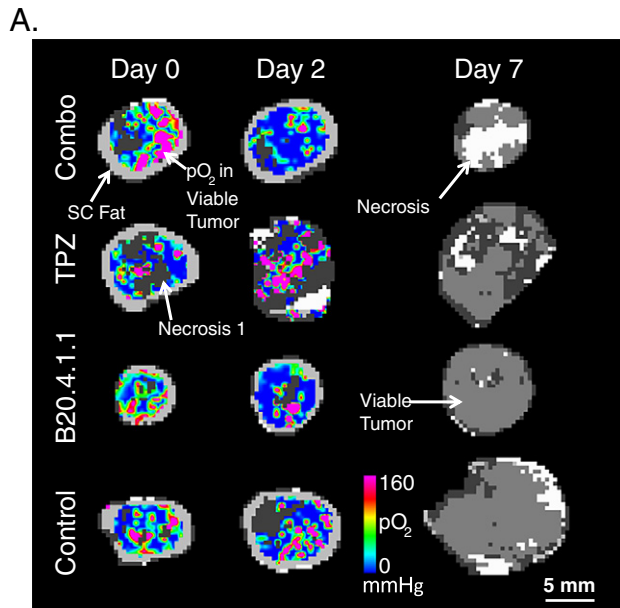


Figure 4. TPZ and B20 treatment significantly increased tumor hypoxia and reduced viable tumor volume. (A) Color-coded viable tumor pO₂ maps are superimposed on the corresponding MS tissue class maps for represented animals from each treatment group (pre and 2 days post treatment). Only the MS tissue class map is shown for Day 7 since pO₂ was not measured on Day 7. The tissue classes found in the MS tissue class map are gray scale encoded as follows: dark gray – necrosis 1; moderate gray – viable tumor; light gray – subcutaneous adipose tissue; white – necrosis 2; viable tumor – underlies the color-coded viable tumor pO₂ map for Day 0 and Day 2. (B) Change in viable tumor pO₂. At Day 2 post treatment, a significant reduction of pO₂ in the viable tumor was seen in B20.4.1.1 and combo groups measured by ¹⁹F-MRI. (C) Percent change in MS viable tumor volume. ##P < .01 relative to pre-treatment level. *P < .05, **P < .01, ***P < .0001, ****P < .0001 with respect to control (Dunnett's).

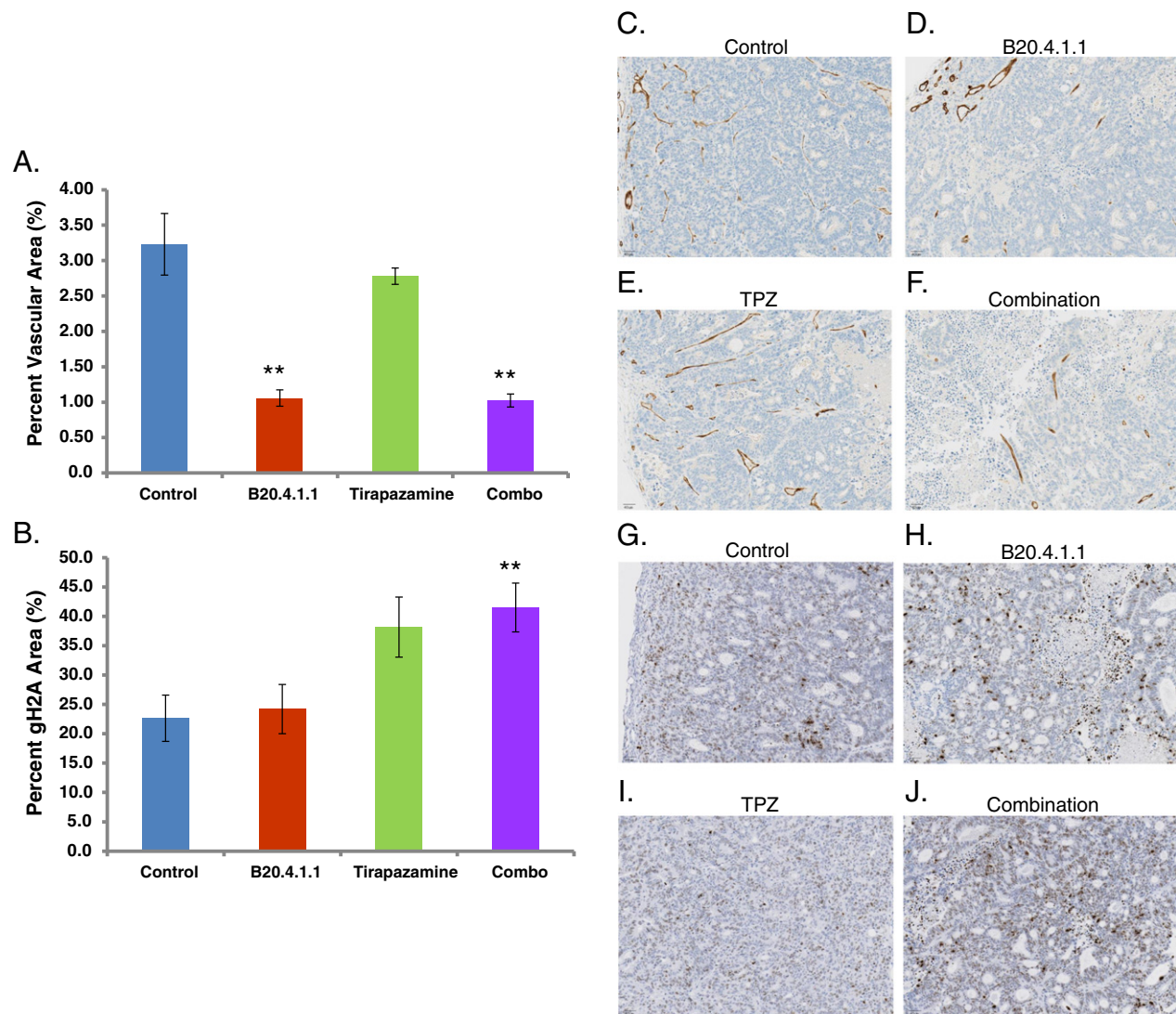


Figure 5. The TPZ and B20.4.1.1 combination treatment significantly decreased vascular density and increased DNA damage in the viable tumor. (A) Percent vascular density. B20.4.1.1 and combo groups showed a significant reduction in percent vascular area. (B) Percent gH2A stained area. The combo group showed a significant increase of gH2A stain positive area. (C-F) Images show MECA-32 stained sections for representative animals from each of the different treatment groups (brown, MECA-32 staining). (G-J) Images show gH2A stained sections for representative animals from each of the different treatment groups. Images depict DNA damage (brown, gH2A staining). ** $P < .01$ with respect to control (Dunnett's).

proved performance over the two monotherapy arms. At present there are now a number of hypoxia-activated drugs at various stages of clinical development [23]. This study provides evidence that clinical trials combining anti-vascular agents and hypoxia-activated prodrugs should be considered to improved efficacy in cancer patients.

Acknowledgements

The authors would like to thank the *in vivo* cell culture team and laboratory animal resources at Genentech for their support of these studies.

References

- [1] Conley SJ, Gheordunescu E, Kakarala P, Newman B, Korkaya H, Heath AN, Clouthier SG, and Wicha MS (2012). Antiangiogenic agents increase breast cancer stem cells via the generation of tumor hypoxia. *Proc Natl Acad Sci U S A* **109**, 2784–2789.
- [2] Mehta S, Hughes NP, Buffa FM, Li SP, Adams RF, Adwani A, Taylor NJ, Levitt NC, Padhani AR, and Makris A, et al (2011). Assessing early therapeutic response to bevacizumab in primary breast cancer using magnetic resonance imaging and gene expression profiles. *J Natl Cancer Inst Monogr* **43**, 71–74.
- [3] Rapisarda A, Hollingshead M, Uranchimeg B, Bonomi CA, Borgel SD, Carter JP, Gehrs B, Raffeld M, Kinders RJ, and Parchment R, et al (2009). Increased antitumor activity of bevacizumab in combination with hypoxia inducible factor-1 inhibition. *Mol Cancer Ther* **8**, 1867–1877.
- [4] Shi Y, Oeh J, Eastham-Anderson J, Yee S, Finkle D, Peale Jr FV, Ross J, Hedeus M, van Bruggen N, and Venook R, et al (2013). Mapping in vivo tumor oxygenation within viable tumor by 19F-MRI and multispectral analysis. *Neoplasia* **15**, 1241–1250.
- [5] Dings RPM, Loren M, Heun H, McNeil E, Griffioen AW, Mayo KH, and Griffin RJ (2007). Scheduling of radiation with angiogenesis inhibitors anginex and avastin improves therapeutic outcome via vessel normalization. *Clin Cancer Res* **13**, 3395–3402.
- [6] Lee CG, Heijn M, di Tomaso E, Griffon-Etienne G, Ancukiewicz M, Koike C, Park KR, Ferrara N, Jain RK, and Suit HD, et al (2000). Anti-vascular endothelial growth factor treatment augments tumor radiation response under normoxic or hypoxic conditions. *Cancer Res* **60**, 5565–5570.
- [7] Myers AL, Williams RF, Ng CY, Hartwich JE, and Davidoff AM (2011). Bevacizumab-induced tumor vessel remodeling in rhabdomyosarcoma xenografts

- increases the effectiveness of adjuvant ionizing radiation. *J Pediatr Surg* **45**, 1080–1085.
- [8] Jain RK (2005). Normalization of tumor vasculature: an emerging concept in antiangiogenic therapy. *Science* **307**, 58–62.
- [9] Harris AL (2002). Hypoxia – a key regulatory factor in tumour growth. *Nat Rev Cancer* **2**, 38–47.
- [10] Wilson WR and Hay MP (2011). Targeting hypoxia in cancer therapy. *Nat Rev Cancer* **11**, 393–410.
- [11] Horsman MR, Mortensen LS, Petersen JB, Busk M, and Overgaard J (2012). Imaging hypoxia to improve radiotherapy outcome. *Nat Rev Clin Oncol* **9**, 674–687.
- [12] De Bock K, Mazzone M, and Carmeliet P (2011). Antiangiogenic therapy, hypoxia, and metastasis: risky liaisons, or not? *Nat Rev Clin Oncol* **8**, 393–404.
- [13] Rapisarda A and Melillo G (2012). Overcoming disappointing results with antiangiogenic therapy by targeting hypoxia. *Nat Rev Clin Oncol* **9**, 378–390.
- [14] Mason RP, Antich PP, Babcock EE, Constantinescu A, Peschke P, and Hahn EW (1994). Noninvasive determination of tumor oxygen-tension and local variation with growth. *Int J Radiat Oncol Biol Phys* **29**, 95–103.
- [15] Dardzinski BJ and Sotak CH (1994). Rapid tissue oxygen-tension mapping using F-19 inversion-recovery echo-planar imaging of perfluoro-15-crown-5-ether. *Magn Reson Med* **32**, 88–97.
- [16] Hunjan S, Zhao DW, Constantinescu A, Hahn EW, Antich PP, and Mason RP (2001). Tumor oximetry: Demonstration of an enhanced dynamic mapping procedure using fluorine-19 echo planar magnetic resonance imaging in the Dunning prostate R3327-AT1 rat tumor. *Int J Radiat Oncol* **49**, 1097–1108.
- [17] Jordan BF, Cron GO, and Gallez B (2009). Rapid monitoring of oxygenation by (19)F magnetic resonance imaging: simultaneous comparison with fluorescence quenching. *Magn Reson Med* **61**, 634–638.
- [18] Kadayakkara DKK, Janjic JM, Pusateri LK, Young W-B, and Ahrens ET (2010). In vivo observation of intracellular oximetry in perfluorocarbon-labeled glioma cells and chemotherapeutic response in the CNS using fluorine-19 MRI. *Magn Reson Med* **64**, 1252–1259.
- [19] Sampath D, Oeh J, Wyatt SK, Cao TC, Koeppen H, Eastham-Anderson J, Robillard L, Ho CCK, Ross J, and Zhuang G, et al (2013). Multimodal microvascular imaging reveals that selective inhibition of Class I PI3K is sufficient to induce an antivascular response. *Neoplasia* **15**, 694–711.
- [20] Brown JM (1993). SR 4233 (tirapazamine): a new anticancer drug exploiting hypoxia in solid tumours. *Br J Cancer* **67**, 1163–1170.
- [21] Hanauke AR, Ross M, Degen D, Hilsenbeck SG, and Von Hoff DD (1993). In vitro activity of the benzotriazine dioxide SR 4233 against human tumour colony-forming units. *Eur J Cancer* **29A**, 423–425.
- [22] Zeman EM, Brown JM, Lemmon MJ, Hirst VK, and Lee WW (1986). SR-4233: a new bioreductive agent with high selective toxicity for hypoxic mammalian cells. *Int J Radiat Oncol Biol Phys* **12**, 1239–1242.
- [23] Phillips RM (2016). Targeting the hypoxic fraction of tumours using hypoxia-activated prodrugs. *Cancer Chemother Pharmacol* **77**, 441–457.
- [24] Carano RAD, Ross AL, Ross J, Williams SP, Koeppen H, Schwall RH, and Van Bruggen N (2004). Quantification of tumor tissue populations by multispectral analysis. *Magn Reson Med* **51**, 542–551.
- [25] Fan XB, River JN, Muresan AS, Popescu C, Zamora M, Culp RM, and Karczmar GS (2006). MRI of perfluorocarbon emulsion kinetics in rodent mammary tumours. *Phys Med Biol* **51**, 211–220.
- [26] Berry LR, Barck KH, Go MA, Ross J, Wu X, Williams SP, Gogineni A, Cole MJ, Van Bruggen N, and Fuh G, et al (2008). Quantification of viable tumor microvascular characteristics by multispectral analysis. *Magn Reson Med* **60**, 64–72.
- [27] Ungersma SE, Pacheco G, Ho C, Yee SF, Ross J, van Bruggen N, Peale Jr FV, Ross S, and Carano RAD (2010). Vessel imaging with viable tumor analysis for quantification of tumor angiogenesis. *Magn Reson Med* **63**, 1637–1647.
- [28] Wang X, Wang T, and Bu J (2011). Color image segmentation using pixel wise support vector machine classification. *Pattern Recogn* **44**, 777–787.
- [29] Hernandez MIQ (2005). School of Computer Science. University of Birmingham; 2005. Ph. D. thesis.
- [30] Veta M, van Diest PJ, Kornegoor R, Huisman A, Viergever MA, and Pluim JP (2013). Automatic nuclei segmentation in H&E stained breast cancer histopathology images. *PLoS One* **8**, e70221.
- [31] Liang WC, Wu X, Peale FV, Lee CV, Meng YG, Gutierrez J, Fu L, Malik AK, Gerber HP, and Ferrara N, et al (2006). Cross-species vascular endothelial growth factor (VEGF)-blocking antibodies completely inhibit the growth of human tumor xenografts and measure the contribution of stromal VEGF. *J Biol Chem* **281**, 951–961.
- [32] O'Connor JPB, Carano RAD, Clamp AR, Ross J, Ho CC, Jackson A, Parker GJ, Rose CJ, Peale FV, and Friesenhahn M, et al (2009). Quantifying antivascular effects of monoclonal antibodies to vascular endothelial growth factor: insights from imaging. *Clin Cancer Res* **15**, 6674–6682.
- [33] Baker JH, Kyle AH, Bartels KL, Methot SP, Flanagan EJ, Balbirnie A, Cran JD, and Minchinton AI (2013). Targeting the tumour vasculature: exploitation of low oxygenation and sensitivity to NOS inhibition by treatment with a hypoxic cytotoxin. *PLoS One* **8**, e76832.